Title

Multi-omic analysis of urothelial cancer patients treated with PD-L1 blockade demonstrates the contribution of both systemic and somatic factors to the biology of response and resistance

Authors

Alexandra Snyder[1]*, Tavi Nathanson[2]*, Samuel Funt[1]*, Arun Ahuja[2], Jacqueline Buros Novik[2], Matthew D. Hellmann[1], Eliza Chang[2], Bulent Arman Aksoy[2], Hikmat Al-Ahmadie[3], Erik Yusko[4], Marissa Vignali[4], Sharon Benzeno[4], Mariel Boyd[1], Meredith Moran[1], Gopa Iyer[1], Harlan S. Robins[4,5], Elaine R. Mardis[6], Taha Merghoub[1], Jeff Hammerbacher[2]^, Jonathan Rosenberg[1]^, Dean Bajorin[1]^

*These authors contributed equally.

^These authors are co-corresponding.

Affiliations:

[1]Department of Medicine, Memorial Sloan Kettering Cancer Center, New York, NY; Department of Medicine, Weill Cornell Medical College, New York, NY 10065

[2]Department of Genetics and Genomic Sciences, Icahn School of Medicine at Mount Sinai, New York, NY 10029

[3]Department of Pathology, Memorial Sloan Kettering Cancer Center, New York, NY 10065

[4]Adaptive Biotechnologies, Seattle, WA 98102

[5]Fred Hutchinson Cancer Research Center, Seattle, Washington 98109

[6]Institute for Genomic Medicine; The Research Institute at Nationwide Children's Hospital; The Ohio State University College of Medicine; Columbus, OH 43205

The authors declare no potential conflicts of interest.

Abstract

Background: Inhibition of programmed death-ligand one (PD-L1) with atezolizumab can induce durable clinical benefit (DCB) in patients with metastatic urothelial cancers, including complete remissions in patients with chemotherapy refractory disease. Although mutation load and PD-L1 immune cell (IC) staining have been associated with response, they lack sufficient sensitivity and specificity for clinical use. Thus, there is a need to evaluate the peripheral blood immune environment and to conduct detailed analyses of mutation load, predicted neoantigens and immune cellular infiltration in tumors to enhance our understanding of the biologic underpinnings of response and resistance.

Methods and Findings: We performed whole exome sequencing (WES), RNA sequencing (RNA-seq), and T cell receptor sequencing (TCR-seq) of pre-treatment tumor samples as well as TCR sequencing of matched, serially collected peripheral blood pre- and post-treatment with atezolizumab. These parameters were assessed for correlation with DCB (defined as progression free survival (PFS) > 6 months) and overall survival (OS), both alone and in the context of clinical and intratumoral parameters known to be predictive of survival in this disease state.

Patients with DCB displayed a higher proportion of tumor infiltrating T lymphocytes (TIL) (n=24, Mann-Whitney p=0.047). Pre-treatment peripheral blood TCR clonality below the median was associated with improved PFS (n=29, log-rank p=0.048) and OS (n=29, log-rank p=0.011). Patients with DCB also demonstrated more substantial expansion of tumor-associated TCR clones in the peripheral blood 3 weeks after starting treatment (n=22, Mann-Whitney p=0.022). The combination of high pre-treatment peripheral blood TCR clonality with elevated PD-L1 IC

staining in tumor tissue was strongly associated with poor clinical outcomes (n=10, HR=86.22, 95% CI (2.55, 491.65)). Marked variations in mutation loads were seen with different somatic variant calling methodologies, which in turn impacted associations with clinical outcomes. Missense mutation load, predicted neoantigen load and expressed neoantigen load did not demonstrate significant association with DCB (n=25, Mann-Whitney p=0.22, n=25, Mann-Whitney p=0.55, and n=25, Mann-Whitney p=0.29 respectively). Instead, we found evidence of time-varying effects of somatic mutation load on progression-free survival in this cohort (n=25, p=0.044).

Conclusions: These results demonstrate the complex nature of immune response to checkpoint blockade and the compelling need for greater interrogation and data integration of both host and tumor factors. Incorporating these variables in prospective studies will facilitate identification and treatment of resistant patients.

Introduction

Atezolizumab has demonstrated responses in 15-25% of patients with advanced urothelial carcinoma and improved survival compared to historical expectations (1,2). Similar to predictive factor analyses in melanoma, colon cancer and non-small cell lung cancer studies with other checkpoint blockade agents, Rosenberg and colleagues reported a statistically significant association between mutation load and response to atezolizumab in urothelial cancer patients (2). However, mutation load in the atezolizumab study was predicted based on an estimate using a targeted panel and not with WES. Similar to findings from prior studies, the association between this predicted mutation load and outcomes in patients with urothelial cancer was not dichotomous; there were tumors from patients with elevated mutation load that did not respond

74 to therapy, and vice versa. Additionally, positive PD-L1 staining of infiltrating immune cells by
75 immunohistochemistry was associated with, but poorly predicted, response. A statistical model
76 suggested that both PD-L1 staining and mutation load impacted the likelihood of response.
77 However, the authors did not recommend its clinical use.

78 Collectively, studies to date imply that a combination of immune parameters are
79 necessary to gain further precision in determining the likelihood of benefit from these
80 immunotherapies and that a single biologic marker will be insufficient. There have been few
81 attempts to integrate molecular and immunologic data from patients treated with checkpoint
82 blockade and their tumors. Consequently we performed whole exome (WES), RNA, and T cell
83 receptor (TCR) sequencing of tumor samples from patients treated with atezolizumab as well as
84 TCR sequencing of matched, serially collected peripheral blood.

85 In this cohort of patients, we illustrate the importance of host immune factors, including
86 intratumoral and peripheral T cell receptor clonality, infiltration and expansion, to clinical
87 outcomes. We did not find a significant association between mutation or expressed neoantigen
88 load and progression free survival or DCB (defined as progression free survival (PFS) > 6
89 months). However, we did demonstrate a time-dependent relationship between mutation load
90 and outcome, implyling that patients who experienced rapid progression displayed systemic
91 indicators of immune deficiency despite elevated mutation load in the tumors. Calculation of the
92 hazard ratios for each measured biomarker and clinical factor underscores the concept that a
93 complex interaction of both host and tumor variables determines whether a patient will
94 experience clinical benefit from anti-PD-L1 therapy.
95

Methods

Patients and clinical characteristics

All patients had locally advanced or metastatic urothelial carcinoma and were treated at Memorial Sloan Kettering Cancer Center (n=29) on protocol NCT02108652 (2). All patients initiated therapy in 2014 and were treated with atezolizumab 1200 mg IV every 3 weeks, and had consented to Institutional Review Board-approved protocols permitting tissue and blood collection and sequencing. Patient tumor samples were assessed prospectively and centrally (by HistoGeneX, Brussels, Belgium) for PD-L1 expression by immunohistochemistry with the SP142 assay (Ventana, AZ, USA) (1). The PD-L1 tumor-infiltrating immune cell (IC) status was defined by the percentage of PD-L1-positive immune cells in the tumor microenvironment: IC0 (<1%), IC1 (≥1% but <5%), and IC2/3 (≥5%) as defined in the original study. Smoking status was evaluated using previously completed self-reported smoking questionnaires or review of medical records.

Tumor and blood samples

All tumor tissue used for sequencing was obtained prior to dosing with atezolizumab. Tumor samples used for whole exome sequencing were all formalin-fixed paraffin embedded (FFPE). The presence of tumor tissue in the sequenced samples was confirmed by examination of a representative hematoxylin and eosin-stained slide by a genitourinary pathologist (H.A.). Peripheral blood mononuclear cells (PBMCs) were isolated and stored as previously described (3). PBMC were collected pre-treatment and during treatment.

118 Clinical efficacy analysis

119 Tumor responses to atezolizumab were evaluated by CT scan every 9 weeks for the first 12
120 months following day 1 of cycle 1. After 12 months, tumor assessments were performed every
121 12 weeks. The response evaluation criteria in solid tumors (RECIST) version 1.1 was used to
122 define objective clinical responses by the institutional radiologist.

123

124 DNA extraction and high-throughput TCRβ Sequencing

125 Genomic DNA was purified from total PBMCs and tumor samples using the Qiagen DNeasy
126 Blood extraction kit. The TCRβCDR3 regions were amplified and sequenced using immunoSEQ
127 (Adaptive Biotechnologies, Seattle, WA) as previously described (4). In brief, bias-controlled V
128 and J gene primers were used to amplify rearranged V(D)J segments for high-throughput
129 sequencing at ~20X coverage. After correcting sequencing errors via a clustering algorithm,
130 CDR3 segments were annotated according to the International ImMunoGeneTics Collaboration
131 (5) to identify the V, D, and J genes that contributed to each rearrangement. A mixture of
132 synthetic TCR analogs in each PCR was used to estimate the absolute template abundance
133 (i.e., the number of cells bearing each unique TCR sequence) from sequencing data, as
134 previously described (6). The estimated TIL content was calculated as previously described (6–
135 8). To determine TIL content in FFPE samples as a T cell fraction, we amplified several
136 housekeeping genes and quantitated their template counts to determine the amount of DNA
137 usable for TCRB sequencing. ImmunoSEQ then amplifies and sequences the molecules with
138 rearranged TCRb chains. Because the immunoSEQ assay aligns sequences to the the IMGT
139 database, sequences are annotated as complete VDJ rearrangements or non-productive
140 rearrangements (a stop codon or out of frame CDR3 region was generated during VDJ
141 recombination in one of the alleles; all downstream analysis in this work proceeded with
142 complete, productive sequences. To estimate the number of starting templates that were in the

143 sample, the number of sequence reads for each TCRB sequences is measured. Synthetic
144 control templates were also spiked into each sample, thereby enabling quantitation of input
145 TCRB templates from the read counts. To determine the proportion of T cells in the FFPE
146 samples, we amplified several housekeeping genes and quantitated their template counts to
147 determine the amount of DNA usable for TCRB sequencing. For each sample, Shannon entropy
148 was also calculated on the clonal abundance of all productive TCR sequences in the data set.
149 Shannon entropy was normalized to the range by dividing Shannon entropy by the logarithm of
150 the number of unique productive TCR sequences in the data set. This normalized entropy value
151 was then inverted (12 normalized entropy) to produce the clonality metric. Those T cell clones
152 whose frequencies differed between samples from a given subject taken at different time points,
153 or between cell populations (e.g., between total PBMCs and tumor) were computationally
154 identified as previously described (9). The input data consisted of the absolute abundance for
155 each TCR clone in each sample. Fisher's exact test was used to compute a p-value for each
156 clone across the two samples, against the null hypothesis that the population abundance of the
157 clone is identical in the two samples. We corrected for multiple testing to control FDR using the
158 Benjamini-Hochberg procedure and employed a significance threshold of 0.01 on adjusted p-
159 values.
160
161 Whole Exome Sequencing
162 Twenty-six FFPE-derived tumor and frozen PBMC-derived normal paired samples were
163 sequenced by exome hybrid capture using the IDT xGen Whole Exome Panel
164 (https://www.idtdna.com/pages/products/nextgen/target-capture/xgen-lockdown-panels/xgen-
165 exome-panel) and standard protocols. Briefly, each sample was used to create a barcoded
166 Illumina library, tumor samples were pooled at optimal multiplex to create an equimolar pool into
167 the hybrid capture reaction, which was performed according to the manufacturer's suggested

168 protocol. Similarly, normal samples were pooled and introduced to the hybrid capture reaction.
169 Following the recovery of captured library fragments, PCR amplification was performed, the
170 resulting pools of fragments were quantitated using qPCR (Kapa Bio), and sequenced in
171 separate lanes by paired end 150 bp reads, using the Illumina HiSeq 4000.
172
173 Somatic Variant Calling
174 DNA sequencing data for the tumor and normal samples were aligned to the GRCh37 reference
175 using bwa-mem (v. 0.7.10) with default settings. The resulting BAMs were processed through
176 Picard MarkDuplicates and the GATK (v. 3.5-0) pipeline including Base Quality Score
177 Recalibration and Indel Realignment. Single nucleotide variants were called from Mutect (v.
178 1.1.6) and Strelka (v. 1.0.14) with default settings. Variants from either call were included and
179 the variants calls were further filtered to those with depth (in normal and tumor samples) ≥ 7
180 reads, > 10% tumor VAF and ≤ 3% normal VAF (10). Mutations per megabase was computed
181 by normalizing the number of mutations by the number of loci with ≥ 7 reads in normal and
182 tumor samples.
183
184 Variants were annotated as missense variants by Varcode (v. 0.5.10,
185 https://github.com/hammerlab/varcode) and PyEnsembl (v. 1.0.3,
186 https://github.com/hammerlab/pyensembl) using Ensembl Release 75 and annotated as
187 deleterious using PolyPhen (v. 2.2.2).

188

189 Mutational signatures were inferred from the somatic mutation calls using *deconstructSigs*.

190

191 HLA typing

192 HLA types for each patient were computed from the normal sequencing data using OptiType (v.

193 1.0.0).

194

195 RNA-seq

196 RNA was extracted from twenty-six FFPE tumor samples and evaluated for quality and quantity

197 using the Agilent RNA pico chip. Each sample was prepared for sequencing by constructing an

198 Illumina Tru-Seq Stranded RNA kit, according to the manufacturer's protocol. The resulting

199 libraries were amplified by PCR, quantitated, pooled and processed through a hybrid capture

200 intermediate using the IDT xGen Exome reagent (as above). The captured fragments were

201 quantitated, diluted and were sequenced using 2 x 150 bp paired end reads on the Illumina

202 HiSeq 4000.

203

204 The RNA sequencing data were aligned to the GRCh37 reference an Ensembl Release 75

205 using STAR (v. 2.4.1d) and transcript quantification was performed using kallisto (v. 0.42.3).

206 The STAR alignment was only used for identifying variant-supporting reads in the RNA. For

207 gene-level analysis, the transcript quantifications were aggregated to the gene level using

208 tximport (http://f1000research.com/articles/4-1521/v1).

209

210 Expressed mutations and neoantigens were computed using Isovar (v. 0.0.6,

211 https://github.com/hammerlab/isovar). This examined the number of RNA reads containing the

212 mutation and the surrounding nucleotide context. Mutations (and neoantigens) were counted as
213 expressed when there were at least 3 reads containing the mutated base.
214
215 sleuth (v. 0.28.1) was used for differential expression analysis and GSEA was used for pathway
216 enrichment analysis. ESTIMATE was used to quantify immune and stromal scores from RNA-
217 seq data.
218
219 Neoantigen calling
220 Neoantigens were computed from all nonsynonymous mutations using Topiary (v. 0.1.0,
221 https://github.com/hammerlab/topiary) and NetMHCCons (v. 1.1) and the computed HLA alleles
222 from OptiType. As with expressed mutations, expressed neoantigens were those supported in
223 the RNA with at least 3 uniquely-mapped reads matching the cDNA sequence.
224
225 Statistical analysis
226 All statistical analysis was performed in Python and R (v. 3.3.1). Cohorts (v. 0.4.0,
227 https://github.com/hammerlab/cohorts) was used to orchestrate the analysis. The Mann Whitney
228 and Fisher's Exact test were performed using the Python scientific computing library, SciPy (v.
229 0.18.1). Kaplan-Meier curves were computed with Lifelines (v. 0.9.1.0). Survival and logistic
230 regression models were estimated using PyStan (v. 2.12.0.0) and the Stan statistical computing
231 software (v. 2.12.0). Survival analyses utilized a proportional hazards piecewise exponential
232 model with a random walk baseline hazard. The analysis for presence of a time-varying
233 covariate effect was performed in R using the *survival* package (v. 2.39.5), whereas the
234 estimation of the time-varying covariate effect was performed using Stan. This analysis
235 estimated the covariate effect at each timepoint with a random-walk prior. In some cases,

236 alternative specifications of models written in Stan were interrogated as sensitivity analyses; see
237 the github repo for details.

238 Results

239 Patient Characteristics

240 29 patients with metastatic urothelial cancer from a single institution treated with atezolizumab
241 as part of a single-arm phase II study (IMvigor 210, NCT 02108652) were included in the
242 analyses. The patients displayed characteristics typical of the metastatic urothelial cancer
243 population studied in IMvigor 210: a preponderance of males with urothelial cancers of bladder
244 origin, greater than half of whom had a reported prior smoking history (Table 1). Patients had an
245 ECOG performance status of 0 or 1, and had 0 to 3 prior regimens of chemotherapy. Of this
246 group, 25 patients had sufficient tumor tissue for WES, 26 for RNA-seq and 24 for TCR-seq. 29
247 had a pre-treatment peripheral blood sample on which TCR-Seq could be performed; 24 had
248 one pre-treatment and at least one post-treatment peripheral blood collection.

249

Table 1: Baseline characteristics		
Variable	Durable Clinical Benefit (n=9)	No Durable Benefit (n=20)
Median Age (range)	66 (57-74)	72 (46-81)
Male Sex	9 (100%)	16 (80%)
Site of primary tumor		
Bladder	7 (78%)	19 (95%)
Upper tract	2 (12%)	1 (5%)
ECOG performance status		

0	0 (0%)	1 (5%)
1	9 (100%)	19 (95%)
History of tobacco use		
No	4 (44%)	7 (35%)
Yes	5 (56%)	13 (65%)
Hemoglobin concentration < 10gm/dL	1 (11%)	3 (15%)
Albumin ≤ lower limit of normal	2 (22%)	5 (25%)
Metastatic sites at baseline		
Visceral^	3 (33%)	16 (80%)
Liver	2 (22%)	9 (45%)
Lymph node only	6 (67%)	4 (20%)
Number of previous systemic regimens in the metastatic setting		
0	5 (56%)	3 (20%)
1	2 (22%)	15 (70%)
2	1 (11%)	1 (5%)
≥ 3	1 (11%)	1 (5%)
Previous neoadjuvant or adjuvant chemotherapy, with first progression within ≤12 months	3 (33%)	2 (10%)
Time since previous chemotherapy ≤ 3 months	2 (29%)	5 (26%)
Prognostic risk group for previously treated patients*		
Low	3 (42%)	7 (37%)
Intermediate	2 (29%)	5 (26%)
High	2 (29%)	7 (37%)
Prognostic risk group for previously untreated patients†		

Low	0 (0%)	0 (0%)
Intermediate	2 (100%)	0 (0%)
High	0 (0%)	1 (100%)
Intravesical BCG administered (%)	2 (22%)	10 (50%)
^Visceral metastasis defined as liver, lung, bone, or any non-lymph node or soft tissue metastasis.*Based on (11) †Based on (12)		

250

251

252

253 Intratumoral and peripheral TCR features associate with durable clinical 254 benefit

255 The importance of T cells to the anti-tumor response has long been known (13); the relevance
256 of intratumoral and peripheral T cell receptor (TCR) clonality to the anti-tumor response is an
257 area of active study. A single previous study of melanoma patients treated with anti-PD-1
258 therapy demonstrated that patients whose tumors featured both high levels of tumor infiltrating T
259 lymphocytes (TIL) along with high TIL clonality were more likely to experience radiographic
260 response to therapy (8). A separate study examined the peripheral TCR repertoire in anti-CTLA-
261 4-treated patients with prostate cancer or melanoma, and found that clonotype stability was
262 associated with response (14). To our knowledge, no prior study has reported both intratumoral
263 and peripheral TCR clonality in a single population treated with checkpoint blockade therapy.
264 We performed TCR sequencing of tumors and peripheral blood mononuclear cells
265 (PBMC) at serial time points in our cohort. Due to limitations in sample availability, this analysis
266 included tumors from 24 patients and peripheral blood from 29 patients, including pre-treatment
267 samples in all patients, and up to 8 total time points. A median of 141,255 (range 43,052-
268 335,089) T cells were analyzed per peripheral blood sample, including 82,636 (range 24,095-

269 207,860) unique TCRs, with a median clonality of 0.080 (range 0.014-0.37) and a median T cell
270 proportion of 0.31 (range 0.082-0.64). In the tumors, the corresponding values included 1,402
271 (range 63-133,167) T cells, 1,086 (range 67-56,273) unique TCRs, clonality of 0.096 (range
272 0.033-0.34) and T cell proportion of 0.097 (range 0.0098-0.33).

273 In our patient group, we first asked whether there was an association between outcome
274 and either tumor TCR clonality or TIL proportion, or with TCR clonality in the peripheral blood.
275 Consistent with the data from Tumeh and colleagues (8), tumors from patients who experienced
276 a DCB exhibited a higher TIL proportion and higher TCR clonality than those patients who
277 experienced progressive disease (Fig 1A, Supplementary Fig S1A). Importantly, TIL proportion
278 alone was also associated with DCB, with a median of 0.21 (range 0.049-0.33) in tumors from
279 patients who had PFS greater than 6 months, versus 0.069 (range 0.0098-0.24) in tumors from
280 patients who did not (n=24, Mann-Whitney p=0.047, Fig 1B); it remains unclear whether TIL
281 clonality adds to TIL proportion in its association with DCB in this study (TIL proportion and
282 clonality versus TIL proportion alone, n=24, log-likelihood p=0.100).
283

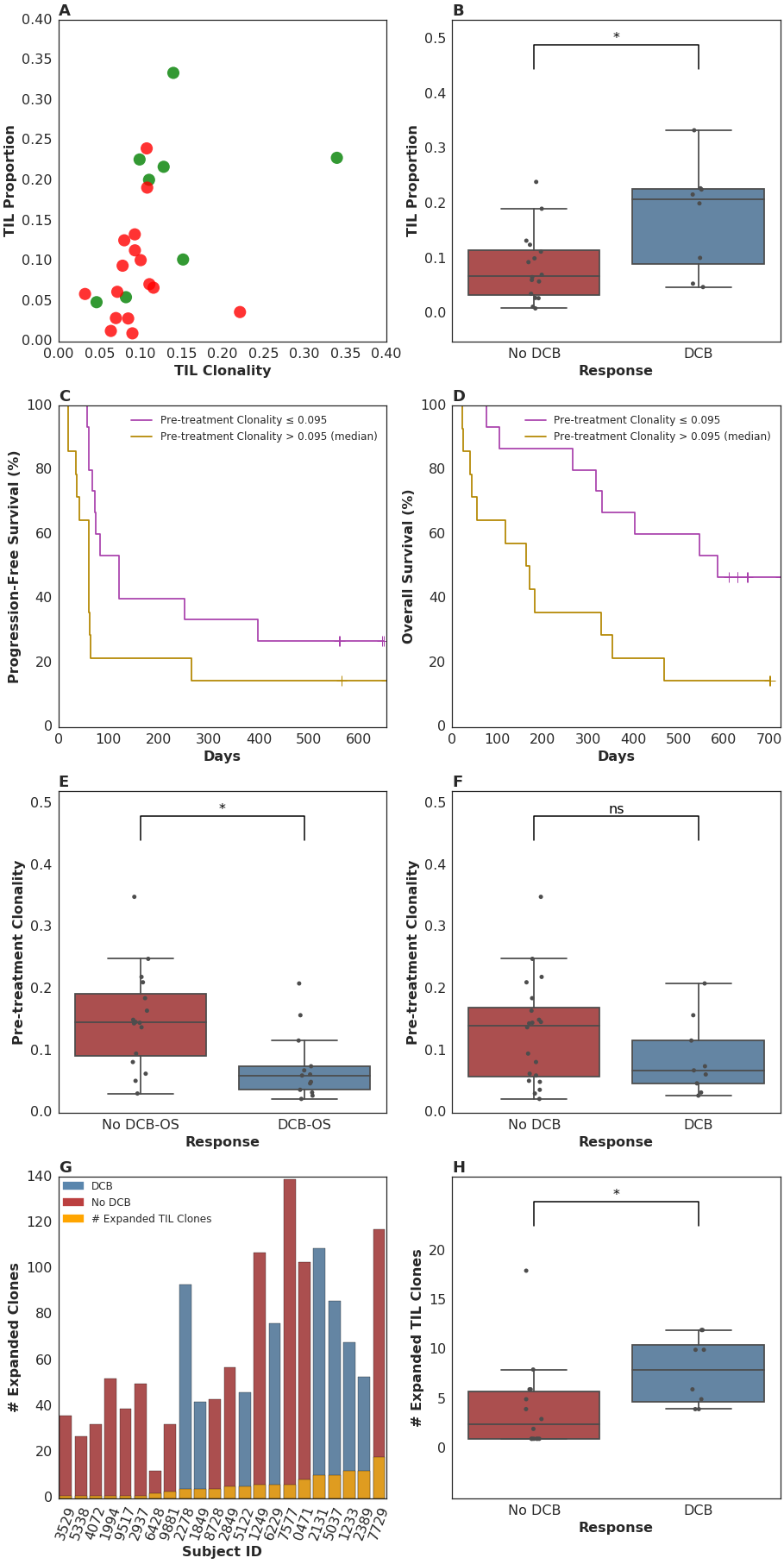
A
TIL Proportion
TIL Clonality
B
TIL Proportion
No DCB
DCB
Response
*
C
Progression-Free Survival (%)
Days
Pre-treatment Clonality ≤ 0.095
Pre-treatment Clonality > 0.095 (median)
D
Overall Survival (%)
Days
Pre-treatment Clonality ≤ 0.095
Pre-treatment Clonality > 0.095 (median)
E
Pre-treatment Clonality
No DCB-OS
DCB-OS
Response
*
F
Pre-treatment Clonality
No DCB
DCB
Response
ns
G
Expanded Clones
DCB
No DCB
Expanded TIL Clones
Subject ID
3529
5338
4072
1994
9517
2937
6428
9881
2278
1849
8728
2849
5122
1249
6229
7577
0471
2131
5037
1233
2389
7729
H
Expanded TIL Clones
No DCB
DCB
Response
*

285 **Fig 1. T-cell receptor clonality and treatment response.**

286 (A) High-throughput quantitative sequencing of the rearranged TCR β genes using the
287 immunoSEQ assay was performed. The x-axis represents clonality of the T-cell repertoire.
288 Absence of DCB (red dots) was associated with lower levels of T-cell infiltration and T-cell
289 clonality than in tumors from patients with DCB (green dots). TIL proportion and TIL clonality
290 were not significantly more predictive of DCB than TIL proportion alone (n=24, log-likelihood
291 p=0.100). (B) TIL proportion alone was associated with DCB, with a median of 0.21 (range
292 0.049-0.33) in tumors from patients who had DCB, versus 0.069 (range 0.0098-0.24) in tumors
293 from patients who did not (n=24, Mann-Whitney p=0.047). (C) Patients with a pre-treatment
294 peripheral TCR clonality less than the median exhibited improved progression free survival
295 (n=29, log-rank p=0.048). (D) Patients with a pre-treatment, peripheral TCR clonality less than
296 the median exhibited improved overall survival (n=29, log-rank p=0.011). (E) There was a
297 significant association between TCR clonality in the peripheral blood prior to initiating treatment
298 and overall survival greater than 12 months (OS DCB, TCR clonality 0.060 (range 0.022-0.21);
299 OS less than 12 months: 0.15 (range 0.031-0.35) (n=29, Mann-Whitney p=0.0061). (F) There
300 was no significant association between pre-treatment peripheral TCR clonality and DCB (DCB,
301 TCR clonality 0.068 (range 0.027-0.21); no DCB: 0.14 (range 0.022-0.35) (n=29, Mann-Whitney
302 p=0.25). (G) Expansion of TCR clones found in the tumor infiltrating T lymphocytes (TIL, orange
303 bars) occurred in the peripheral blood 3 weeks after initiating treatment in all patients. (H) The
304 number of TCR clones found in TIL that expanded in the peripheral blood 3 weeks after initiating
305 treatment was 8.00 (range 4.00-12.00) in patients with DCB and 2.50 (range 1.00-18.00) in non-
306 DCB patients (n=22, Mann-Whitney p=0.022).

307

308 We next examined pre-treatment peripheral blood clonality and its relationship to DCB.
309 Because a diverse TCR repertoire in circulation may increase the likelihood that a tumor specific

310 T cell population is present, we hypothesized that T cell receptor clonality would be inversely
311 associated with response. Indeed, low pre-treatment peripheral TCR clonality associated with
312 improved PFS (n=29, log-rank p=0.048) and OS (n=29, log-rank p=0.011) (Figs 1C, 1D, 1E),
313 although not with DCB (Fig 1F).

314 Finally, we explored the relationship between intratumoral and peripheral TCR clonality.
315 Variations in individual T cell clones present in tumors can be tracked in the peripheral blood
316 during treatment (examples in Supplementary Fig S1B). Expansion of tumor-associated TCRs
317 occurred in the peripheral blood in all patients (Fig 1G). However, a more pronounced
318 expansion of intratumoral TCR clones was observed in DCB patients at three weeks after
319 initiation of treatment (second dose of therapy) (Fig 1H) that diminished by 6 weeks after
320 therapy initiation (Supplementary Fig S1C). Interestingly, all patients with low pre-treatment
321 peripheral TCR clonality and high TIL clonality survived greater than one year (Supplementary
322 Fig S1D).
323

324 Association of tumor genetic features with progression free or overall 325 survival

326 To further examine intratumoral factors associated with therapeutic efficacy, we performed WES
327 on 25 formalin fixed, paraffin-embedded (FFPE) archived tumor samples. Mean target coverage
328 was 129 (range 44-194) in tumors, and 73 (range 59-91) in normal tissue. Single nucleotide
329 variants were identified and annotated as silent, missense or nonsense mutations (Fig 2A).
330 There was no significant association between median missense mutation load and DCB
331 (median mutations per megabase 3.24 (range 0.038-11.46) in patients with DCB compared to
332 0.45 (range 0.019-9.90) in those without DCB, n=25, Mann-Whitney p=0.22, Fig 2B). There was

333 also no significant association between missense mutation load and overall survival greater
334 than 12 months (n=25, Mann-Whitney p=0.37, Supplementary Fig S2A). In a survival analysis
335 for time to disease progression or mortality, the estimated hazard ratio associated with increase
336 in missense SNV count per megabase was 0.92 (95% CI 0.78 - 1.09). These results are not
337 surprising given that the present sample size (n=25) is underpowered to detect an effect of
338 magnitude similar to that observed by Rosenberg and colleagues (2) (power=0.2 assuming
339 median of 12.4 vs 6.4 mutations per megabase among patients with DCB vs non-DCB
340 response).
341

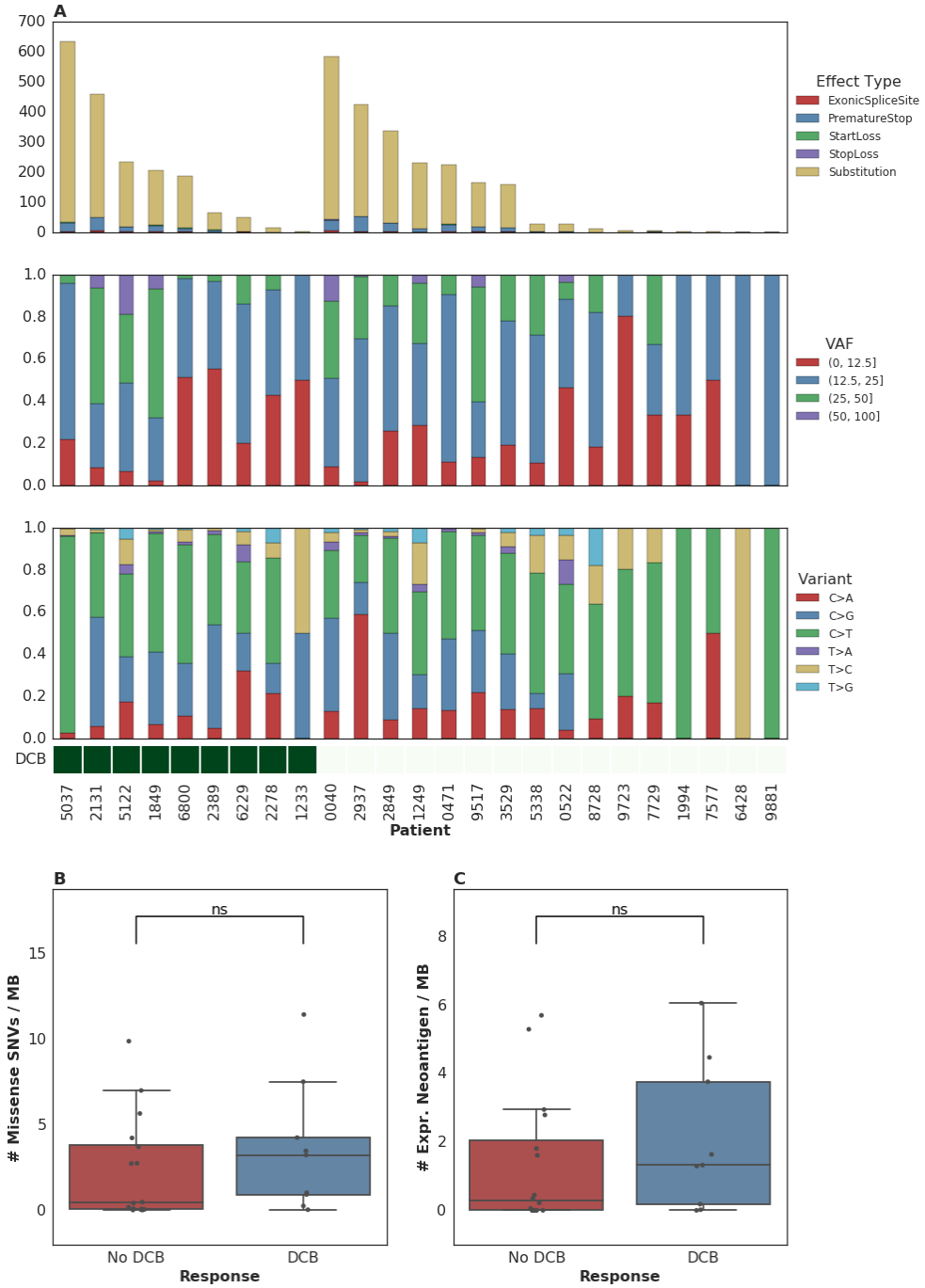

Fig 2. Single nucleotide variants and treatment response.

(A) Single nucleotide variants, premature stop codons, transversions, mutations in start or stop codons and splice site variants as well as transitions and transversions were called for all samples. (B) Median mutations per megabase of 3.24 (range 0.038-11.46) in tumors from

347 patients who progressed at or after 6 months, as compared to 0.45 (range 0.019-9.90) in those
348 who progressed in less than 6 months (n=25, Mann-Whitney p=0.22). (C) Median expressed
349 neoantigens in tumors from patients who progressed at or after 6 months was 1.32 (range 0.00-
350 6.06), versus 0.29 (range 0.00-5.70) in those who progressed before 6 months (n=25, Mann-
351 Whitney p=0.29).
352
353 When filtering to expressed mutations, we found a median of 0.79 (range 0.00-3.36)
354 expressed mutations per megabase for patients with DCB and a median of 0.16 (range 0.00-
355 3.34) expressed mutations per megabase for patients without DCB (n=25, Mann-Whitney
356 p=0.26, Supplementary Fig S2B). Consistent with known importance of specific variant calling
357 pipelines to output (15,16), we found that different filtering techniques impacted the association
358 with DCB (Supplementary Table S1). Missense mutation load, when counting only mutations
359 that were removed after post-processing (via Base Quality Score Recalibration (BQSR) and
360 depth/variant allele frequency (VAF) filtering), was predictive of response (n=25, Mann-Whitney
361 p=0.0078).
362 One hypothesis for explaining the association between mutation load and outcome to
363 treatment with checkpoint blockade is the generation of neoantigens, altered peptides presented
364 by the major histocompatibility complex that are capable of eliciting an anti-tumor T cell
365 response and are more common with increased mutation load. After performing *in silico* HLA
366 typing (Methods), we examined predicted neoantigens that are 8 to 11 amino acids in length
367 resulting from the nonsynonymous mutations of patients treated with atezolizumab. There was
368 no significant association between predicted neoantigens per megabase and either DCB or 12
369 month overall survival. Patients with DCB had a median 4.58 (range 0.037-39.48) predicted
370 neoantigens per megabase while patients without DCB had 1.35 (range 0.00-20.22) (n=25,
371 Mann-Whitney p=0.55, Supplementary Figs 2C, 2D). Filtering of predicted neoantigens to focus

372 only on those expressed in RNA (Methods) also demonstrated no significant association
373 between expressed predicted neoantigens and clinical benefit with atezolizumab (n=25, Mann-
374 Whitney p=0.29, Fig 2C and Supplementary Fig S2B). Again, we acknowledge the limitations in
375 statistical power to detect associations due to the sample size of our study.
376

377 Impact of mutation load on response likelihood increases over time

378 Given that the mutation load and outcomes were weakly associated in the complete IMvigor210
379 dataset and not statistically significantly associated in this cohort, we embarked upon an
380 exploration of additional factors, including tumor microenvironmental and systemic measures,
381 which may modify the importance of this variable or independently impact outcomes.
382 To this end, we examined the time-varying impact of mutation load on PFS to see if
383 mutation load had a differential impact on early hazards in contrast to late hazards. We found
384 evidence of time-varying effects of somatic mutation load on progression-free survival in this
385 cohort (n=25, p=0.044 for association of scaled Schoenfeld residuals with log(time)). There was
386 little association of somatic mutation load with mortality or disease progression in the first 3
387 months (n=25, HR=0.91, 95% CI (0.75, 1.07); Fig 3A). In contrast, there was a notable
388 association of somatic mutation load with clinical events occurring more than 3 months after
389 treatment (n=11, HR=0.69, 95% CI (0.38, 0.99)). When a similar analysis was performed for
390 time-varying association with OS, the evidence in support of time-varying effects was similar
391 (n=25, p=0.082, Fig 3B). Among patients who survived longer than 3 months, the number of
392 somatic mutations per megabase was associated with a lower risk of mortality (n=11, HR=0.80,
393 95% CI (0.60, 1.00)) than during the first three months (n=25, HR=1.02, 95% CI (0.79, 1.22), Fig
394 3B). There was, however, weak evidence in support of a threshold at 3 months after follow-up.

395 In a nonparametric analysis, we found that the reduction in risk associated with somatic
396 mutation load increased steadily over time (Figs 3C, 3D, 3E).

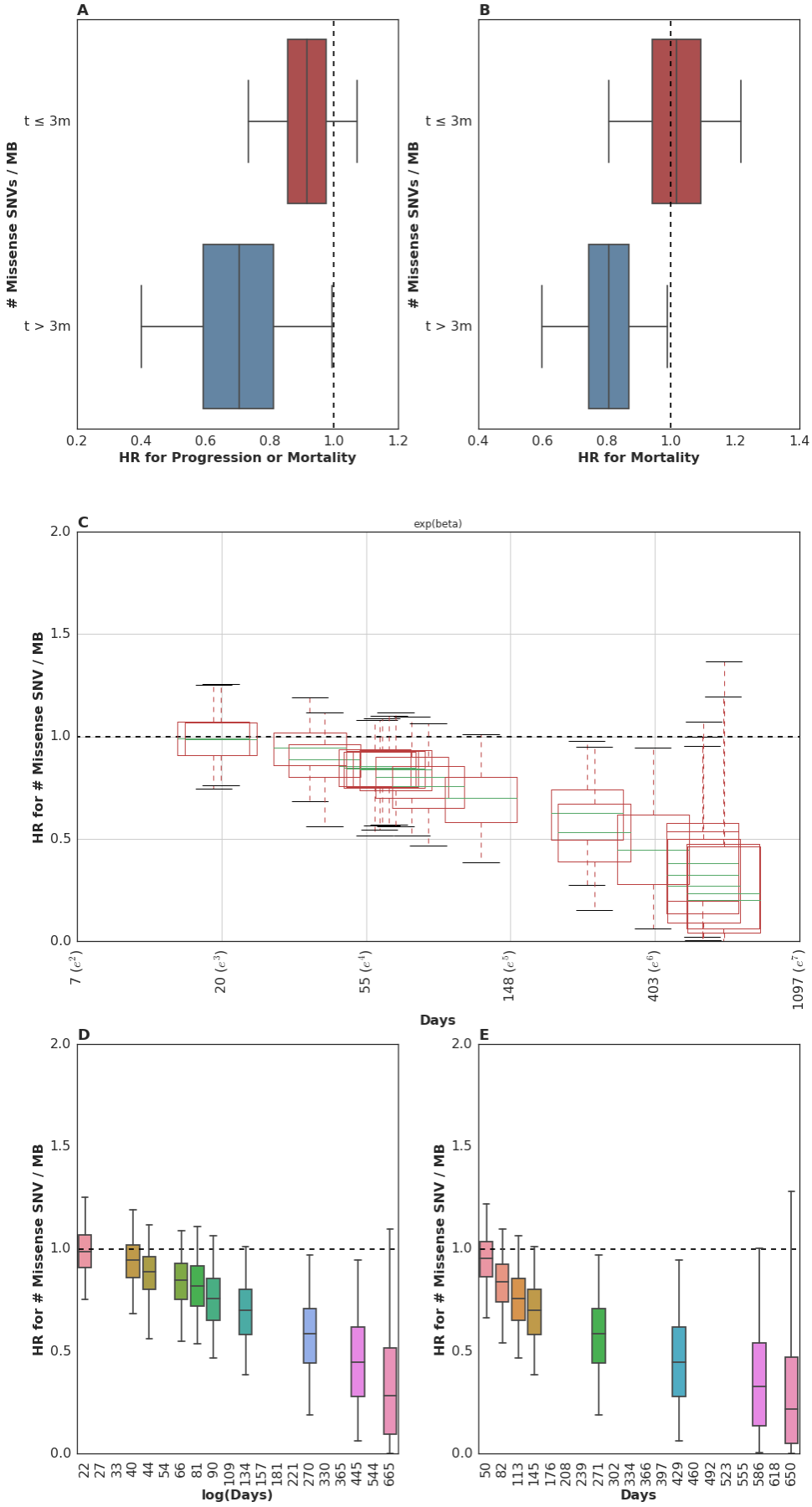
A
t ≤ 3m
t > 3m
Missense SNVs / MB
0.2
0.4
0.6
0.8
1.0
1.2
HR for Progression or Mortality
B
t ≤ 3m
t > 3m
Missense SNVs / MB
0.4
0.6
0.8
1.0
1.2
1.4
HR for Mortality
C
exp(beta)
HR for # Missense SNV / MB
2.0
1.5
1.0
0.5
0.0
7 (e^2)
20 (e^3)
55 (e^4)
148 (e^5)
403 (e^6)
1097 (e^7)
Days
D
HR for # Missense SNV / MB
22 27 33 40 44 54 66 81 90 109 134 157 181 221 270 330 365 445 544 665
log(Days)
E
HR for # Missense SNV / MB
50 82 113 145 176 208 239 271 302 334 366 397 429 460 492 523 555 586 618 650
Days

397

398 **Fig 3. Time dependent relationship between mutation load and treatment response.**
399 (A) There was no significant association between somatic mutation load and PFS for events
400 occurring in the first 3 months (red box: HR=0.91, 95% CI (0.75, 1.07)), as compared to those
401 more than 3 months following therapy (blue box: HR=0.69, 95% CI (0.38, 0.99)). (B) There was
402 no significant association between somatic mutation load and OS for events occurring in the first
403 3 months (red box: HR=1.02, 95% CI (0.79, 1.22)), as compared to those more than 3 months
404 following therapy (blue box: HR=0.80, 95% CI (0.60, 1.00)). (C) The hazard ratio for each
405 mutation per megabase, estimated at each unique failure time. Red box plots summarize 50%
406 and 95% posterior intervals for each observed failure/censor time, with median values shown in
407 green. Time (Days) is plotted on a log-scale. Estimates are not independent from one another
408 since the model utilizes a random-walk parameterization to allow the variance in hazard over
409 time to be modeled flexibly. (D) Summary of estimated change in hazard for disease
410 progression or death with each observed mutation per megabase, reported as exp(beta) or
411 Hazard Ratios. Estimates here are reported per interval of failure time, with failure times
412 segmented at regular intervals of log(time) since therapy. Boxplots depict 50% and 95%
413 posterior intervals for hazard ratio at each interval, with median values shown with horizontal
414 lines. Intervals with no boxplot are those during which no failure or censor events were
415 observed. Note that these estimates are not independent from one another since the model
416 utilizes a random-walk parameterization to allow the variance in hazard over time to be modeled
417 flexibly. (E) Summary of estimated change in hazard for disease progression or death with each
418 observed mutation per megabase, reported as exp(beta) or Hazard Ratios. Estimates here are
419 reported per interval of failure time, with failure times segmented at regular intervals of days
420 since therapy. Boxplots depict 50% and 90% posterior intervals for hazard ratio at each interval,
421 with median estimates shown as horizontal lines. Intervals with no boxplot are those during
422 which no failure or censor events were observed. Note that these estimates are not independent

423 from one another since the model utilizes a random-walk parameterization to allow the variance
424 in hazard over time to be modeled flexibly.
425
426 These data suggest that in patients with rapidly progressive disease, factors other than
427 mutation load likely determine their outcome. This observation is not surprising in that clinical
428 factor analysis of this disease state has identified a heterogeneous population of patients, with 5
429 clinical factors distinguishing those likely to experience a rapid and early death from those more
430 likely to survive longer (11). We hypothesized that such patients might simply be too clinically
431 and systemically unwell to mount the necessary immune response, despite some of them
432 harboring tumor biomarkers thought to confer a likelihood of DCB, including elevated mutation
433 load. When we examined the 5-factor score in this subset relative to the rest of the dataset, we
434 found that indeed patients who survived less than or equal to 3 months exhibited a significantly
435 higher 5-factor score (3.00 (range 2.00-4.00), in contrast to 1.50 (range 0.00-4.00) in patients
436 who survived longer than 3 months (n=26, Mann-Whitney p=0.018, Supplementary Fig S3A).
437 Patients surviving less than 3 months were much more likely to have liver metastases: 100% in
438 patients surviving less than or equal to 3 months and 22% in patients surviving longer than 3
439 months (n=29, Fisher's Exact p=0.00097, Supplementary Fig S3B). There were no significant
440 differences in these patients with respect to BCG exposure (n=29, Fisher's Exact p=0.20),
441 missense SNV load (n=25, Mann-Whitney p=0.26) and pre-treatment peripheral TCR clonality
442 (n=29, Mann-Whitney p=0.12). These data suggest that there is a subset of nearly end-stage
443 patients with cancer in whom clinical variables may negate immunological response despite the
444 presence of one or more favorable tumor-associated biomarkers. The inclusion of these clinical
445 variables is warranted in future studies.
446

447 ## Examination of the tumor microenvironment shows evidence for adaptive
448 immunity and suppression in responding tumors

449 Several studies have suggested that an “inflamed” tumor microenvironment, tumor or immune
450 cell PD-L1 expression increase the likelihood of response to checkpoint blockade. As seen in
451 the published IMVigor 210 cohort, PD-L1 IC expression was significantly associated with DCB in
452 this subset (n=29, Spearman rho=0.48 p=0.0083, Supplementary Fig S4A). We quantified
453 immune infiltration from RNA-seq using ESTIMATE (17). The immune score, while associated
454 with the TIL proportion estimated through TCR Seq (Supplementary Fig S4B), was estimated to
455 be 764.37 (range -1195.08-1509.65) in patients with DCB and 263.49 (range -1100.78-1734.28)
456 in patients without DCB but was not significantly different (n=26, Mann-Whitney p=0.33,
457 Supplementary Fig S4C). When we performed gene set enrichment analysis (GSEA) using the
458 Hallmark Geneset (18), we did not observe any differentially expressed gene sets between
459 tumors from patients with DCB versus no DCB. Furthermore, RNA expression of *PD-L1* did not
460 correlate with reported immune cell PD-L1 staining level (n=26, Spearman rho=0.045 p=0.83,
461 Supplementary Fig S4D). We did not observe a difference in tumor MHC class I expression
462 according to DCB (Supplementary Fig S4E, *HLA-A*: n=26, Mann-Whitney p=0.26, *HLA-B*: n=26,
463 Mann-Whitney p=0.36, *HLA-C*: n=26, Mann-Whitney p=0.24).

464 Given that such agnostic approaches did not reveal a clear association between tumor
465 microenvironment factors and response, we pursued a hypothesis-driven approach examining
466 the genes that show upregulation at the cell surface during T cell exhaustion. When categorized
467 by DCB, there was no significant difference in expression of such genes, including *CTLA-4,*
468 *TIGIT, HAVCR2 (TIM-3)* or *LAG-3* (19). When grouped by PD-L1 staining, we found low
469 expression of all markers in the PD-L1 low group (IC0), as expected. However, in the PD-L1
470 high group (IC2), *HAVCR* exhibited significantly higher expression in tumors from patients who

experienced DCB than in those who did not (Supplementary Fig S4F). Interestingly, of the three IC2 tumors, two had missense SNV loads significantly below the median (17 and 57); the third had 412 SNVs. Additionally, although Rosenberg and colleagues (2) found that among the four TCGA subtypes of RNA expression, luminal cluster II showed a significantly higher response rate, no significant association was found here between the four clusters and DCB (n=20, Fisher's Exact p=0.36) (Supplementary Fig S4G), nor between the luminal/basal sub-categorization and DCB (n=20, Fisher's Exact p=1.00), possibly due to sample size.

Relative importance of somatic, immune, and clinical factors in resistance and response to PD-L1 blockade

Unanswered questions that arise from the many studies of biomarker correlates of checkpoint blockade response are whether measures such as mutation load, PD-L1 staining, and others reflect the same “tumor state,” or if each confers an independent effect on outcome?

When examined in conjunction with mutation load, the greater the expression of PD-L1, the more negative the association of mutation load with hazard (i.e. higher mutation load was associated with longer survival). Among patients with tumors showing little-to-no expression of PD-L1 (IC0 rated), each unit increase in missense SNV count per megabase was associated with a negligible change in hazard (n=4, HR=1.43, 95% CI (0.75, 2.98)). Among patients with tumors expressing PD-L1 at moderate or high levels (IC1 or IC2 staining), missense SNV count per megabase was associated with lower risk for disease progression or mortality (among IC1: n=11, HR=0.75, 95% CI (0.47, 1.14); among IC2: n=10, HR=0.73, 95% CI (0.48, 1.06)). Although our limited sample size precludes making an assertion that mutation load is associated with survival in any particular subgroup (e.g. when looking among IC1 and IC2 tumors alone); our data do support the presence of an interaction among these variables (p=0.046 for

494 interaction; Supplementary Fig S5A). Given the plausibility of the finding that somatic mutation
495 load may correlate better with survival among patients with an inflamed tumor
496 microenvironment, the addition of somatic mutation load to PD-L1 IC staining warrants further
497 study.

498 We found a similar albeit weaker interaction effect when looking at association of
499 somatic mutation load (missense SNV count per megabase) and progression-free survival
500 according to the presence/absence of liver metastasis prior to treatment administration (p=0.14
501 for interaction). Among patients without liver metastasis, somatic mutation load was associated
502 with a lower risk for disease progression or mortality (n=16, HR=0.73, 95% CI (0.50, 1.02),
503 Supplementary Fig S5B) than patients with liver metastasis (n=9, HR=0.96, 95% CI (0.66, 1.37),
504 Supplementary Fig S5B).

505 To our surprise, although both PD-L1 staining and mutation load were each associated
506 with response in the original study (2) these variables did not correlate with each other (Fig 4A).
507 Furthermore, pre-treatment peripheral TCR clonality did not correlate with mutation load (Fig
508 4B). The lack of association between these variables suggests that each might confer an
509 independent or semi-independent impact on the likelihood of response to therapy. TCR clonality
510 and infiltration did, however, correlate with PD-L1 IC score: those tumors with higher clonality or
511 higher infiltration also featured higher PD-L1 staining (p=0.02 and p=0.01, respectively, Figs 4C,
512 4D).

513

514

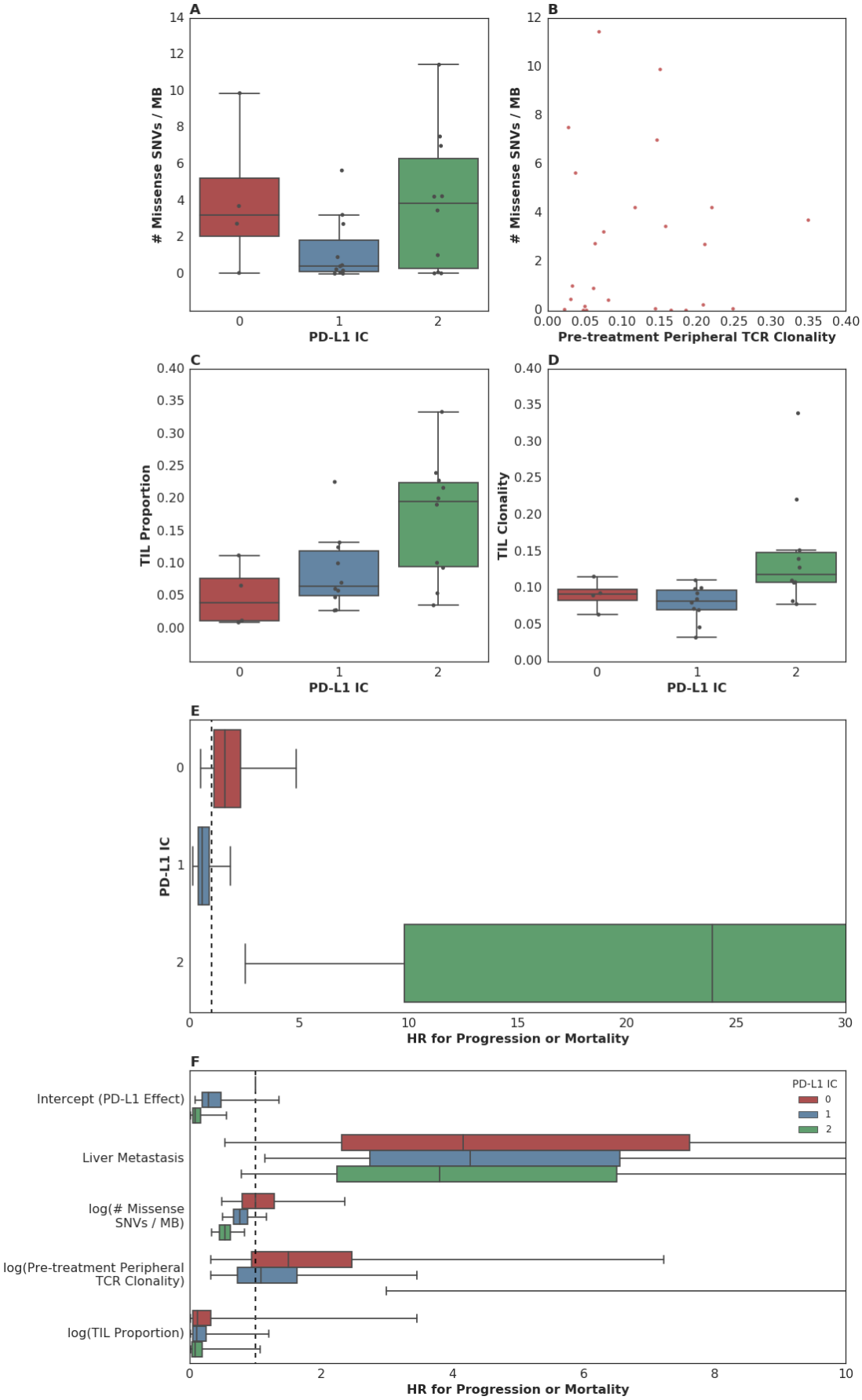
A
Missense SNVs / MB
PD-L1 IC
B
Missense SNVs / MB
Pre-treatment Peripheral TCR Clonality
C
TIL Proportion
PD-L1 IC
D
TIL Clonality
PD-L1 IC
E
PD-L1 IC
HR for Progression or Mortality
F
Intercept (PD-L1 Effect)
Liver Metastasis
log(# Missense SNVs / MB)
log(Pre-treatment Peripheral TCR Clonality)
log(TIL Proportion)
PD-L1 IC
0
1
2
HR for Progression or Mortality

516 **Fig 4. Associations between measured somatic, immune and clinical variables.**
517 (A) Although both PD-L1 staining and mutation load each were weakly associated with
518 response, these variables were not correlated with each other (n=25, Spearman rho=0.14
519 p=0.51). (B) Pre-treatment peripheral TCR clonality did not correlate with mutation load (n=25,
520 Pearson r=0.0017 p=0.99). (C) TIL proportion as estimated by TCR sequencing was associated
521 with PD-L1 IC staining (n=24, Spearman rho=0.51 p=0.010). (D) TIL clonality was associated
522 with PD-L1 IC staining (n=24, Spearman rho=0.48 p=0.017). (E) Hazard associated with
523 log(pre-treatment peripheral TCR clonality) by level of immune cell PD-L1 expression (IC0, IC1
524 or IC2). (F) Multivariate survival analysis of various clinical, peripheral and intratumoral
525 biomarkers for association with time to disease progression or mortality (PFS), utilizing a
526 varying-coefficient model which allows the hazard associated with a one-unit increase in a
527 biomarker's value to vary according to level of intratumoral PD-L1 expression (IC score).
528
529 In an analysis to see whether the association between pre-treatment peripheral TCR
530 clonality and progression-free survival varied by PD-L1 IC score, we found some evidence of an
531 interaction (p=0.015 for interaction; Fig 4E). Among patients with low levels of PD-L1
532 expression, there was little association between pre-treatment peripheral TCR clonality and
533 progression-free survival (among IC0: n=4, HR=1.87, 95% CI (0.49, 4.86); among IC1: n=11,
534 HR=0.69, 95% CI (0.14, 1.85)). Among patients with high levels of PD-L1 expression, by
535 comparison, we observed almost complete separation of progression-free survival according to
536 pre-treatment peripheral TCR clonality (among IC2: n=10, HR=86.22, 95% CI (2.55, 491.65);
537 Fig 4E). Similar results were seen in analyses with respect to OS, and in a logistic regression
538 analysis for DCB (Supplementary Figs 5C, 5D, 5E).
539 To resolve the hypothesis that those patients with low peripheral TCR clonality simply
540 were healthier, we examined the association between 5-factor score and pre-treatment

541 peripheral TCR clonality and did not find such an association (n=26, Spearman rho=0.25
542 p=0.22, Supplementary Fig S5F).
543 In a multivariate survival model for time to disease progression or mortality, which allows
544 the effect of each biomarker to vary according to intratumoral PD-L1 IC score, we find that the
545 correlation of each intratumoral, peripheral or clinical biomarker with disease progression or
546 mortality is relatively independent of the others (Fig 4F, Supplementary Fig S5G). Perhaps with
547 the notable exception of the impact of liver metastatic status on time to progression or survival,
548 the correlation of each intratumoral or peripheral biomarker with outcome is strongest in the
549 group with the highest levels of immune cell PD-L1 expression (Supplementary Table S2).
550

551 # Discussion

552 The treatment of previously incurable metastatic solid tumors with checkpoint blockade agents
553 has led to dramatic success in a minority of patients, a finding that has generated substantial
554 excitement in the field, with associated correlative studies and drug development. Despite such
555 studies, a deeper understanding of the biology of response and resistance is often eclipsed by
556 the search for biomarkers. Of the multitude of studied biomarkers, to date, PD-L1 staining
557 (either tumor cell or immune cell) and mutation load have emerged as the most consistently
558 positive predictors of response to checkpoint blockade (10,20,21). However, in all studies the
559 exceptions are patients who benefit despite having tumors with low mutation load or who lack
560 high PD-L1 staining, which demonstrates the inadequacy of these biomarkers in excluding and
561 therefore denying a patient with limited or no treatment options access to potentially life-saving
562 therapy.

563 Here, we undertook the in-depth characterization of tumors and peripheral blood from 29
564 patients treated on IMvigor 210, a Phase II study in which 310 patients were treated with the
565 anti-PD-L1 agent atezolizumab. Although the overall study found significant associations
566 between mutation load as measured by the Foundation Medicine targeted sequencing panel
567 and radiographic response (2), there was no statistically significant association between
568 mutation load and durable clinical benefit or survival in the patient subset studied here, despite
569 the similarity of our study population to the parent study. This contrast may be due to a
570 combination of factors. First, though statistically significant, the association in the overall study
571 was not categorical: as in other studies of mutation load, this factor alone was not predictive of
572 response. Second, we have less power to detect this association in our smaller subset
573 compared with the larger studied cohort. Third, standardized definitions and calculations of
574 mutation load do not exist as yet; each published study has used differing methodologies
575 (2,10,20,21). Indeed, in this study, depending on the method used, the association between
576 mutation load and clinical outcomes varied from $p<0.08$ to $p>0.4$ (AUCs and p-values in
577 Supplementary Table S1). To illustrate the fickle nature of defining mutation load, counting only
578 the mutations excluded by BQSR, as opposed to only those remaining after BQSR, showed a
579 significant association with DCB. Together, these findings underscore the need for improved
580 and standardized mutation calling methods. The weak association of mutation load with DCB
581 and the lack of such standardization render this biomarker unfit for application to individual
582 patients at present. Furthermore, the time-dependent relationship between mutation load and
583 survival implies that a clinical and immunological state may exist in patients with advanced
584 cancer, such that patients with very rapidly progressing disease and expected death in <3
585 months do not respond despite the presence of positive biomarkers.

586 In an attempt to deepen our understanding of the biology of response and resistance, we
587 studied additional factors: immune factors, conveyed here as peripheral and intratumoral TCR

588 clonality and TIL proportion; and systemic factors such as the 5-factor score and presence of
589 liver metastases. We found that even in this small dataset, TCR clonality below the median in
590 the peripheral blood prior to treatment, expansion of tumor-associated TCR in the periphery 3
591 weeks after initiating treatment, and higher TIL proportion all associated with clinical benefit.
592 These data suggest that TCR sequencing provided additional insights into response and
593 resistance beyond mutation load and PD-L1 staining. With respect to biomarker development,
594 our study implies that non-invasive metrics such as pre-treatment peripheral TCR clonality and
595 known prognostic features such as the presence of liver metastases may be worthy of further
596 study in urothelial cancer patients treated with PD-L1 blockade.

597 Finally, though limited in power by the small sample size, we attempted to integrate the
598 importance of the studied variables. This analysis demonstrated both hypothesized and
599 unexpected interactions. For example, while mutation burden seemed to associate with
600 outcome more significantly in PD-L1 IC1 and-2 tumors, high PD-L1 IC staining in the setting of
601 high peripheral TCR clonality was associated with a substantial hazard for poor outcome. Given
602 the significance of PD-L1 expression in mediating response to anti-PD-L1 therapy, the presence
603 of these interactions may argue in their favor as predictive rather than prognostic biomarkers.
604 Further analysis is required to elucidate the role of these biomarkers in mediating response to
605 checkpoint blockade.

606 In conclusion, we have demonstrated that to truly understand and ultimately circumvent
607 resistance to checkpoint blockade, we must pursue integrated studies of the somatic, immune
608 and systemic features of each treated patient.

609

610

611

612

613 Acknowledgements: Carol Aghajanian and Jedd Wolchok for their mentorship of AS.

614

615 Funding: This work was supported by the Ludwig Center for Cancer Research and the NIH/NCI

616 Cancer Center Support Grant P30 CA008748.

617

618 Supplementary Information, Captions

619 Supplementary Tables

620 Supplementary Table S1. Choice of depth and VAF filtering, as well as whether or not to run

621 Base Quality Score Recalibration (BQSR), resulted in differences in predictive value for

622 mutation load. We chose to optimize for precision, choosing the highlighted set of filters/BQSR.

623 Precision is defined as the fraction of filtered missense mutations in IMPACT genes that were

624 actual IMPACT panel variants. Recall is defined as the fraction of actual IMPACT panel variants

625 that were found in the filtered missense results.

626

627 Supplementary Table S2. Summary of results from multivariate survival analysis of various

628 clinical, peripheral and intratumoral factors to estimate their independent association with

629 hazard for disease progression or mortality (PFS) and for mortality (OS) according to level of

630 intratumoral PD-L1 expression (IC grade). Results are summarized as median and 95%

631 posterior intervals.

632

633 # Supplementary Figures

634 Supplementary Fig S1A. Tumors with less than the median TIL proportion or clonality were less
635 likely to display DCB (25%, versus no DCB: 81%, n=24, Fisher's Exact p=0.021).
636
637 Supplementary Fig S1B. TCR overlap between the pre-treatment and 3-week posttreatment
638 peripheral blood in one patient with limited clinical benefit (PFS=37 days) and one patient with
639 durable clinical benefit (CR at 630 days after starting treatment). The association between pre-
640 treatment peripheral blood TCR sequences (x axis) and posttreatment peripheral blood TCR
641 sequences (y axis) is overlaid with the presence of tumor associated T cell clones. Gray
642 indicates TCRs present only in the peripheral blood; blue indicates TCRs present in the tumor
643 and blood; orange indicates TCRs present in the tumor and expanded in the blood with
644 treatment.
645
646 Supplementary Fig S1C. There was no significant expansion of TIL-associated TCR clones
647 between pre-treatment (3.00 (range 1.00-9.00)) and 6 weeks post-treatment (2.00 (range 1.00-
648 8.00)), n=20, Mann-Whitney p=0.17.
649
650 Supplementary Fig S1D. The combination of high pre-treatment TIL and low pre-treatment
651 peripheral blood TCR clonality were predictive of DCB (n=24, Fisher's Exact p=0.0069) and
652 DCB-OS (n=24, Fisher's Exact p=0.014). For DCB, a logit model combining both was more
653 predictive than peripheral blood (n=24, log-likelihood p=0.00029) or TIL (n=24, log-likelihood
654 p=0.00051) clonality alone. For DCB-OS, both combined were more predictive than TIL (n=24,
655 log-likelihood p=0.0029) clonality alone.
656

657 Supplementary Fig S2A. No significant association between the number of missense SNV per
658 megabase and overall survival, with 2.13 (range 0.038-11.46) in tumors from those patients who
659 survived greater than 12 months, versus 0.48 (range 0.019-9.90) in those who did not (n=25,
660 Mann-Whitney p=0.37).
661
662 Supplementary Fig S2B. No significant difference between median expressed neoantigens in
663 tumors from patients who survived greater than or equal to 12 months: was 1.31 (range 0.00-
664 6.06), versus 0.35 (range 0.00-5.30) in those who survived less than 12 months (n=25, Mann-
665 Whitney p=0.36).
666
667 Supplementary Fig S2C. No significant difference between median predicted neoantigens per
668 megabase: 4.58 (range 0.037-39.48) in tumors from patients with DCB, as compared to 1.35
669 (range 0.00-20.22) in those who progressed in less than 6 months (no DCB) (n=25, Mann-
670 Whitney p=0.55).
671
672 Supplementary Fig S2D. No significant difference between median predicted neoantigens per
673 megabase in tumors from those patients who survived greater than 12 months (here used to
674 define OS DCB) was 3.56 (range 0.037-39.48) as compared to 1.37 (range 0.00-20.22) in those
675 who did not (no DCB) (n=25, Mann-Whitney p=0.81).
676
677 Supplementary Fig S3A. Patients who survived less than 3 months (red box) exhibited a
678 significantly higher 5-factor score (3.00 (range 2.00-4.00), as compared to 1.50 (range 0.00-
679 4.00) in patients who survived >3mo (blue box) (n=26, Mann-Whitney p=0.018).
680

681 Supplementary Fig S3B. Patients who survived less than or equal to 3 months (red box) were
682 more likely to have liver metastases (100% in patients who survived less than or equal to 3
683 months and 22% in patients who survived longer than 3 months, n=29, Fisher's Exact
684 p=0.00097).
685
686 Supplementary Fig S4A. PD-L1 IC staining as reported by the sponsor in the published study
687 (2) and outcome in our cohort were significantly associated in this sub-study (n=29, Spearman
688 rho=0.48 p=0.0083).
689
690 Supplementary Fig S4B. ImmuneScore was associated with TIL proportion (n=24, Spearman
691 rho=0.47 p=0.022).
692
693 Supplementary Fig S4C. There was no association between ImmuneScore and DCB (DCB,
694 764.37 (range -1195.08-1509.65); no DCB 263.49 (range -1100.78-1734.28) (n=26, Mann-
695 Whitney p=0.33).
696
697 Supplementary Fig S4D. PD-L1 expression as measured by RNA-seq was not associated with
698 PD-L1 IC level (n=26, Spearman rho=0.045 p=0.83). Tumor cell PD-L1 staining was not
699 available.
700
701 Supplementary Fig S4E. HLA Class I expression was not associated with DCB (HLA-A: n=26,
702 Mann-Whitney p=0.26, HLA-B: n=26, Mann-Whitney p=0.36, HLA-C: n=26, Mann-Whitney
703 p=0.24).
704

705 Supplementary Fig S4F. Expression of other inhibitory markers, in particular *HAVCR2* (also
706 known as *TIM-3*) was higher in DCB patients in the IC2 group.
707
708 Supplementary Fig S4G. No association was found between TCGA RNA Subtype and response
709 in this sub-study (n=20, Fisher's Exact p=0.36).
710
711 Supplementary Fig S5A. Hazard associated with log(missense SNV count per megabase) by
712 level of immune cell (IC0, IC1 or IC2) PD-L1 expression.
713
714 Supplementary Fig S5B. Hazard associated with log(missense SNV count per megabase) by
715 presence or absence of liver metastasis at enrollment.
716
717 Supplementary Fig S5C. Association of peripheral TCR clonality prior to treatment with time to
718 mortality (OS) varies according to immune cell (IC0, IC1 or IC2) PD-L1 expression.
719
720 Supplementary Fig S5D. Association of peripheral TCR clonality prior to treatment with DCB
721 varies according to immune cell (IC0, IC1 or IC2) PD-L1 expression.
722
723 Supplementary Fig S5E. Association of peripheral TCR clonality prior to treatment with DCB
724 (OS) varies according to immune cell (IC0, IC1 or IC2) PD-L1 expression.
725
726 Supplementary Fig S5F. There was no significant relationship between 5-Factor score and pre-
727 treatment TCR clonality (n=26, Spearman rho=0.25 p=0.22).
728

729 Supplementary Fig S5G. Multivariate survival analysis of various clinical, peripheral and
730 intratumoral biomarkers for association with time to mortality (OS), utilizing a varying-coefficient
731 model which allows the hazard associated with a one-unit increase in a biomarker's value to
732 vary according to level of intratumoral PD-L1 expression (IC score). Note that the x-axis has
733 been truncated at a value of 10 for clarity even though this results in the exclusion of some
734 estimated HR values (specifically that for pre-treatment peripheral TCR clonality among IC2
735 patients).
736
737 Supplementary Fig S6A. No significant association between the number of missense SNV found
738 on MSK-IMPACT and DCB (DCB 0.13 (range 0.00-0.31) versus no DCB 0.046 (range 0.00-
739 0.37) (n=25, Mann-Whitney p=0.42).
740
741 Supplementary Fig S6B. No significant association between the number of missense SNV found
742 on MSK-IMPACT and overall survival (survival greater than 12 months 0.093 (range 0.00-0.31),
743 versus less than 12 months 0.074 (range 0.00-0.37) (n=25, Mann-Whitney p=0.78).
744
745 Supplementary Fig S6C. There was no significant difference in APOBEC signature found in
746 tumors from patients with PFS DCB (0.19 (range 0.00-0.56)) as compared to no DCB (0.00
747 (range 0.00-0.46)) (n=25, Mann-Whitney p=0.23).
748
749 Supplementary Fig S6D. There was a significant correlation between missense SNV count and
750 APOBEC signature mutations (n=25, Pearson r=0.40 p=0.048).
751
752 Supplementary Fig S6E. There was no significant association between FGFR3 mutations or
753 expression (n=26, Mann-Whitney p=0.39).

754

755 Supplementary Fig S6F. There was no significant association between MYC expression and
756 outcome measured by PFS DCB (n=26, Mann-Whitney p=0.87).

757

758 Supplementary Fig S6G. There was no significant association between DNA damage response
759 (DDR) mutations rated as “possible” by PolyPhen and DCB (n=25, Mann-Whitney p=0.20).

760

761 Supplementary Fig S6H. Univariate association of exonic SNV, missense SNV and neoepitope
762 load with DCB, with (blue bars) and without (red bars) filtering by expression.

763

764 Supplementary Fig S6I. Univariate association of exonic SNV, missense SNV and neoepitope
765 load with OS greater than 12 months, with (blue bars) and without (red bars) filtering by
766 expression.

767

768 Supplementary Fig S6J. Univariate association of exonic SNV, missense SNV and neoepitope
769 load with PFS, showing results with (blue bars) and without (red bars) filtering by expression.

770

771 Supplementary Fig S6K. Univariate association of exonic SNV, missense SNV and neoepitope
772 load with OS, showing results with (blue bars) and without (red bars) filtering by expression.

773

774 Supplementary Fig S6L. Univariate association of expressed/total ratio for exonic SNV,
775 missense SNV, and neoantigen loads with PFS.

776

777 Supplementary Fig S6M. Univariate association of expressed/total ratio for exonic SNV,
778 missense SNV, and neoantigen loads with OS.

779

780 Supplementary Fig S6N. Univariate association of expressed/total ratio for exonic SNV,
781 missense SNV, and neoantigen loads with DCB (PFS greater than 12 months).
782
783 Supplementary Fig S6O. Univariate association of expressed/total ratio for exonic SNV,
784 missense SNV, and neoantigen loads with OS greater than 12 months.
785
786 Supplementary Fig S6P. There was no significant association between pack years of reported
787 smoking history and DCB (n=29, Mann-Whitney p=0.87).
788
789 Supplementary Fig S6Q. There were significant associations between PFS (n=29, log-rank
790 p=0.024) and OS (n=29, log-rank p=0.018) and the presence of liver metastasis.
791
792 Supplementary Fig S6R. There was a significant association between the presence of visceral
793 metastases and poor overall survival (n=29, log-rank p=0.020).
794
795 Supplementary Fig S6S. There was not a significant association between 5-factor score and OS
796 (n=26, log-rank p=0.13).
797
798 Supplementary Fig S6T. No significant association between the number of expressed missense
799 SNV per megabase and DCB (DCB 0.79 (range 0.00-3.36), versus no DCB: 0.16 (range 0.00-
800 3.34)), n=25, Mann-Whitney p=0.26.
801

802 # References

803 1. Powles T, Eder JP, Fine GD, Braiteh FS, Loriot Y, Cruz C, et al. MPDL3280A (anti-PD-L1)
804 treatment leads to clinical activity in metastatic bladder cancer. Nature.
805 2014;515(7528):558–62.

806 2. Rosenberg JE, Hoffman-Censits J, Powles T, van der Heijden MS, Balar AV, Necchi A, et
807 al. Atezolizumab in patients with locally advanced and metastatic urothelial carcinoma who
808 have progressed following treatment with platinum-based chemotherapy: a single-arm,
809 multicentre, phase 2 trial. Lancet. 2016;387(10031):1909–20.

810 3. Postow MA, Yuan J, Kitano S, Lesokhin AM, Wolchok JD. Markers for anti-cytotoxic T-
811 lymphocyte antigen 4 (CTLA-4) therapy in melanoma. Methods Mol Biol. 2014;1102:83–95.

812 4. Robins HS, Campregher PV, Srivastava SK, Wacher A, Turtle CJ, Kahsai O, et al.
813 Comprehensive assessment of T-cell receptor beta-chain diversity in alphabeta T cells.
814 Blood. 2009 Nov 5;114(19):4099–107.

815 5. Lefranc M-P, Giudicelli V, Duroux P, Jabado-Michaloud J, Folch G, Aouinti S, et al. IMGT®,
816 the international ImMunoGeneTics information system® 25 years on. Nucleic Acids Res.
817 2015 Jan;43(Database issue):D413–22.

818 6. Wu D, Emerson RO, Sherwood A, Loh ML, Angiolillo A, Howie B, et al. Detection of
819 minimal residual disease in B lymphoblastic leukemia by high-throughput sequencing of
820 IGH. Clin Cancer Res. 2014 Sep 1;20(17):4540–8.

821 7. Hsu MS, Sedighim S, Wang T, Antonios JP, Everson RG, Tucker AM, et al. TCR
822 Sequencing Can Identify and Track Glioma-Infiltrating T Cells after DC Vaccination. Cancer
823 Immunol Res. 2016 May;4(5):412–8.

824 8. Tumeh PC, Harview CL, Yearley JH, Shintaku IP, Taylor EJM, Robert L, et al. PD-1
825 blockade induces responses by inhibiting adaptive immune resistance. Nature. 2014 Nov
826 27;515(7528):568–71.

827 9. DeWitt WS, Emerson RO, Lindau P, Vignali M, Snyder TM, Desmarais C, et al. Dynamics
828 of the cytotoxic T cell response to a model of acute viral infection. J Virol. 2015
829 Apr;89(8):4517–26.

830 10. Rizvi, N., Hellmann, M, Snyder, Et al A. Mutational Landscape Determines Sensitivity to
831 Programmed Cell Death-1 Blockade in Non-Small Cell Lung Cancer. Science. 2015;

832 11. Sonpavde G, Pond GR, Rosenberg JE, Bajorin DF, Choueiri TK, Necchi A, et al. Improved
833 5-Factor Prognostic Classification of Patients Receiving Salvage Systemic Therapy for
834 Advanced Urothelial Carcinoma. J Urol. 2016;195(2):277–82.

835 12. Bajorin DF, Dodd PM, Mazumdar M, Fazzari M, McCaffrey JA, Scher HI, et al. Long-term

836 survival in metastatic transitional-cell carcinoma and prognostic factors predicting outcome
837 of therapy. J Clin Oncol. 1999 Oct;17(10):3173–81.

838 13. Dunn GP, Old LJ, Schreiber RD. The immunobiology of cancer immunosurveillance and
839 immunoediting. Immunity. 2004;21(2):137–48.

840 14. Cha E, Klinger M, Hou Y, Cummings C, Ribas A, Faham M, et al. Improved survival with T
841 cell clonotype stability after anti-CTLA-4 treatment in cancer patients. Sci Transl Med.
842 2014;6(238):238ra70.

843 15. Alioto TS, Buchhalter I, Derdak S, Hutter B, Eldridge MD, Hovig E, et al. A comprehensive
844 assessment of somatic mutation detection in cancer using whole-genome sequencing. Nat
845 Commun. 2015 Dec 9;6:10001.

846 16. Qiu P, Pang L, Arreaza G, Maguire M, Chang KC, Marton MJ, et al. Data Interoperability of
847 Whole Exome Sequencing (WES) Based Mutational Burden Estimates from Different
848 Laboratories. Int J Mol Sci [Internet]. 2016;17(5). Available from:
849 http://dx.doi.org/10.3390/ijms17050651

850 17. Bindea G, Mlecnik B, Tosolini M, Kirilovsky A, Waldner M, Obenauf AC, et al.
851 Spatiotemporal dynamics of intratumoral immune cells reveal the immune landscape in
852 human cancer. Immunity. 2013;39(4):782–95.

853 18. Liberzon A, Subramanian A, Pinchback R, Thorvaldsdottir H, Tamayo P, Mesirov JP.
854 Molecular signatures database (MSigDB) 3.0. Bioinformatics. 2011;27(12):1739–40.

855 19. Tirosh I, Izar B, Prakadan SM, Wadsworth MH 2nd, Treacy D, Trombetta JJ, et al.
856 Dissecting the multicellular ecosystem of metastatic melanoma by single-cell RNA-seq.
857 Science. 2016;352(6282):189–96.

858 20. Van Allen EM, Miao D, Schilling B, Shukla SA, Blank C, Zimmer L, et al. Genomic
859 correlates of response to CTLA-4 blockade in metastatic melanoma. Science.
860 2015;350(6257):207–11.

861 21. Snyder A, Makarov V, Merghoub T, Yuan J, Zaretsky JM, Desrichard A, et al. Genetic basis
862 for clinical response to CTLA-4 blockade in melanoma. N Engl J Med. 2014;371(23):2189–
863 99.

864 22. Forbes SA, Beare D, Gunasekaran P, Leung K, Bindal N, Boutselakis H, et al. COSMIC:
865 exploring the world's knowledge of somatic mutations in human cancer. Nucleic Acids Res.
866 2015 Jan;43(Database issue):D805–11.

867 23. Rosenthal R, McGranahan N, Herrero J, Taylor BS, Swanton C. DeconstructSigs:
868 delineating mutational processes in single tumors distinguishes DNA repair deficiencies
869 and patterns of carcinoma evolution. Genome Biol. 2016 Feb 22;17:31.

870

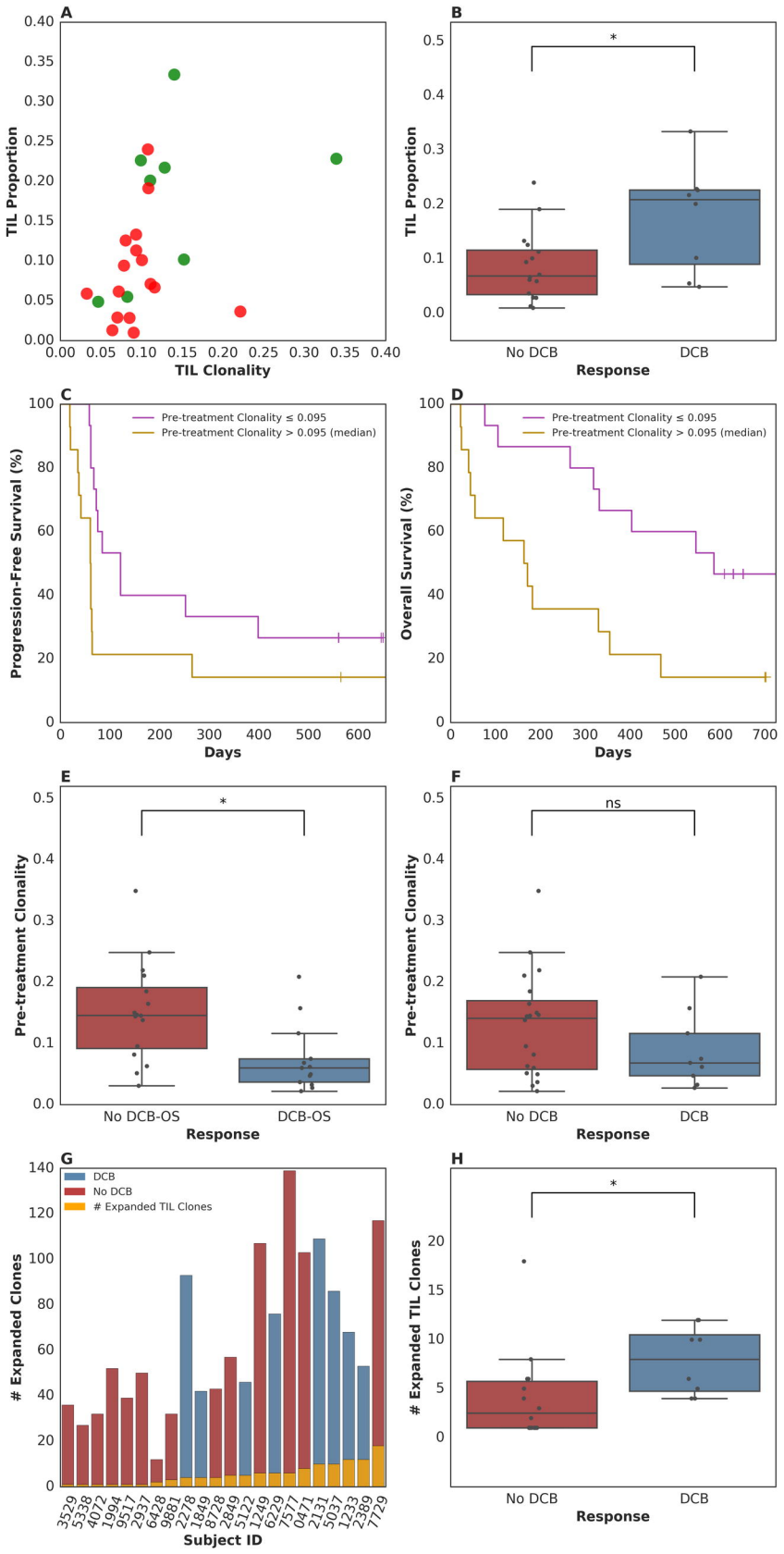
A
TIL Proportion
TIL Clonality
B
*
TIL Proportion
No DCB
DCB
Response
C
Pre-treatment Clonality ≤ 0.095
Pre-treatment Clonality > 0.095 (median)
Progression-Free Survival (%)
Days
D
Pre-treatment Clonality ≤ 0.095
Pre-treatment Clonality > 0.095 (median)
Overall Survival (%)
Days
E
*
Pre-treatment Clonality
No DCB-OS
DCB-OS
Response
F
ns
Pre-treatment Clonality
No DCB
DCB
Response
G
DCB
No DCB
Expanded TIL Clones
Expanded Clones
3529
5338
4072
1994
9517
2937
6428
9881
2278
1849
8728
2849
5122
1249
6229
7577
0471
2131
5037
1233
2389
7729
Subject ID
H
*
Expanded TIL Clones
No DCB
DCB
Response

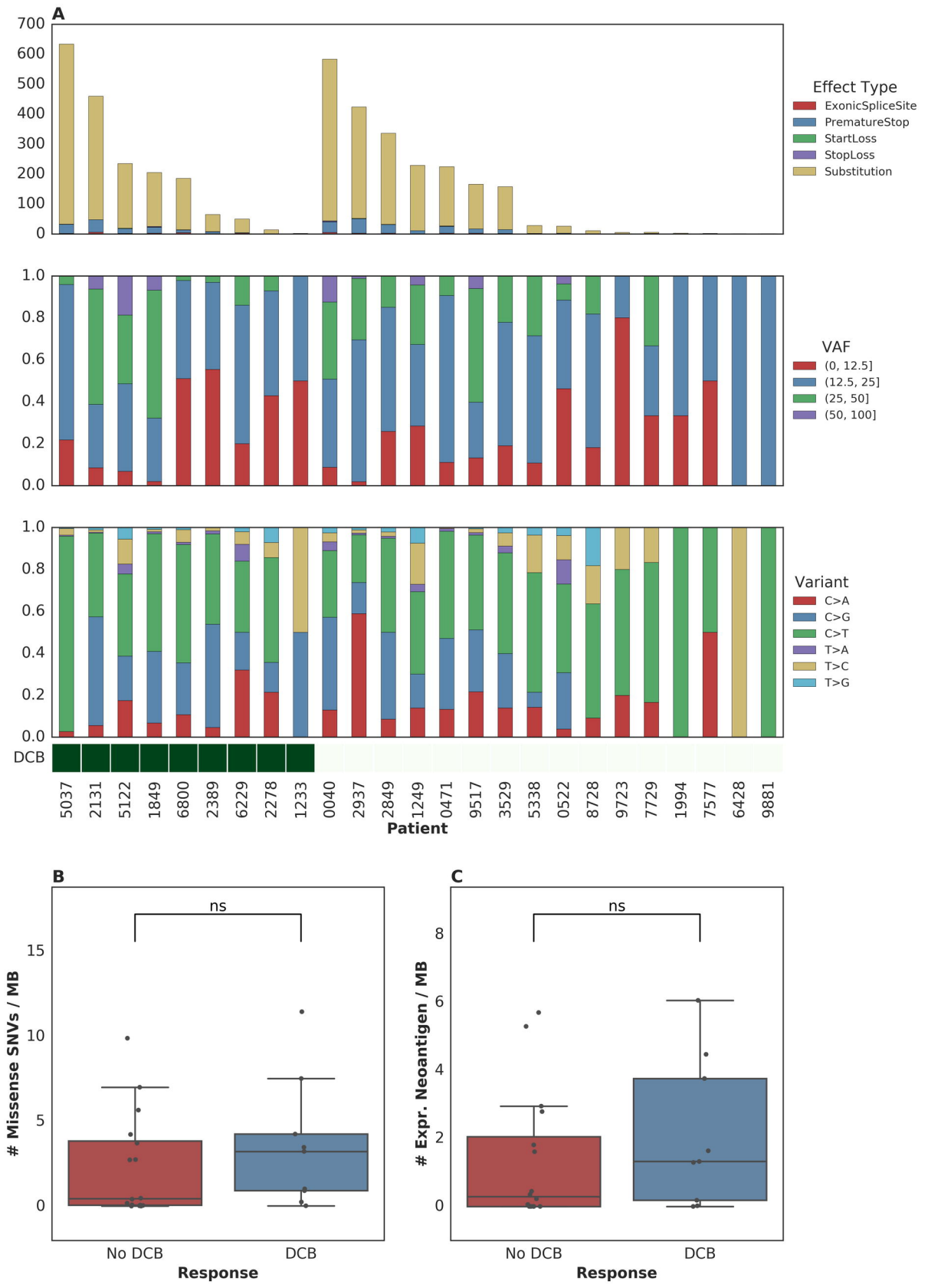
A
Effect Type
ExonicSpliceSite
PrematureStop
StartLoss
StopLoss
Substitution
VAF
(0, 12.5]
(12.5, 25]
(25, 50]
(50, 100]
Variant
C>A
C>G
C>T
T>A
T>C
T>G
DCB
5037
2131
5122
1849
6800
2389
6229
2278
1233
0040
2937
2849
1249
0471
9517
3529
5338
0522
8728
9723
7729
1994
7577
6428
9881
Patient
B
ns
Missense SNVs / MB
No DCB
DCB
Response
C
ns
Expr. Neoantigen / MB
No DCB
DCB
Response

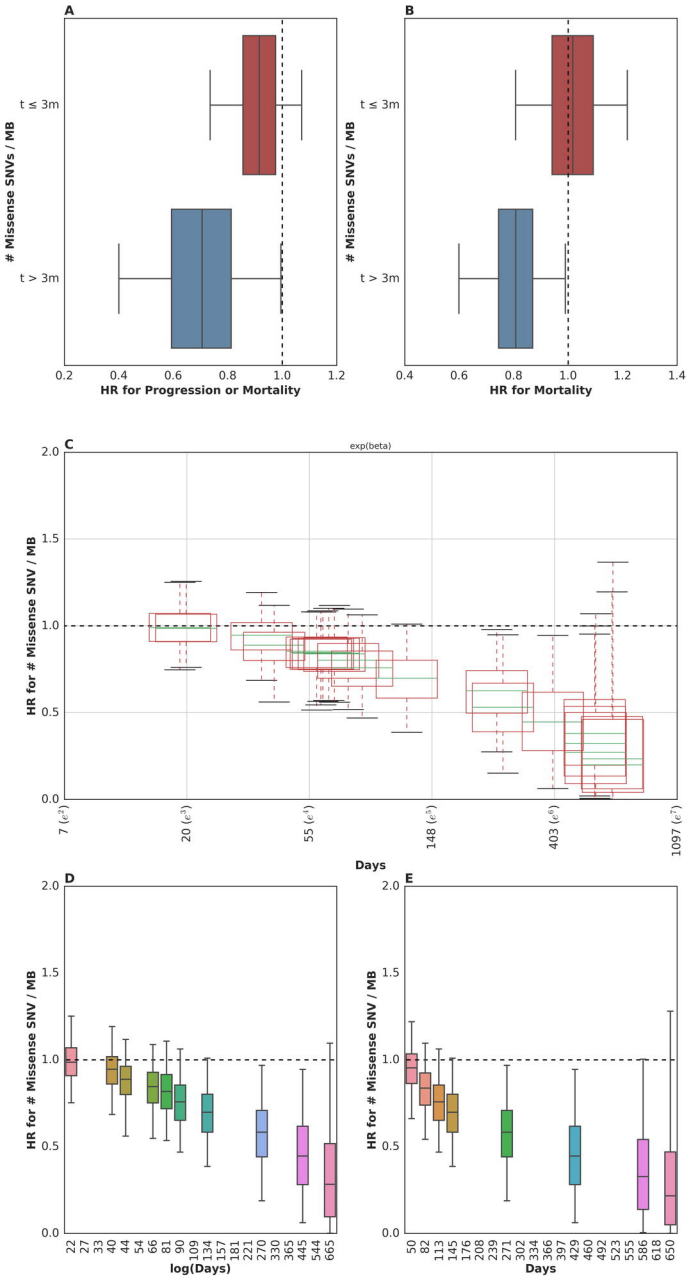
A
Missense SNVs / MB
t ≤ 3m
t > 3m
0.2
0.4
0.6
0.8
1.0
1.2
HR for Progression or Mortality
B
Missense SNVs / MB
t ≤ 3m
t > 3m
0.4
0.6
0.8
1.0
1.2
1.4
HR for Mortality
C
exp(beta)
HR for # Missense SNV / MB
2.0
1.5
1.0
0.5
0.0
7 (e^{2})
20 (e^{3})
55 (e^{4})
148 (e^{5})
403 (e^{6})
1097 (e^{7})
Days
D
HR for # Missense SNV / MB
2.0
1.5
1.0
0.5
0.0
22
27
33
40
44
54
64
81
91
109
134
157
181
221
270
330
365
445
544
665
log(Days)
E
HR for # Missense SNV / MB
2.0
1.5
1.0
0.5
0.0
50
82
113
145
176
208
239
271
302
334
366
397
429
460
492
523
555
586
618
650
Days

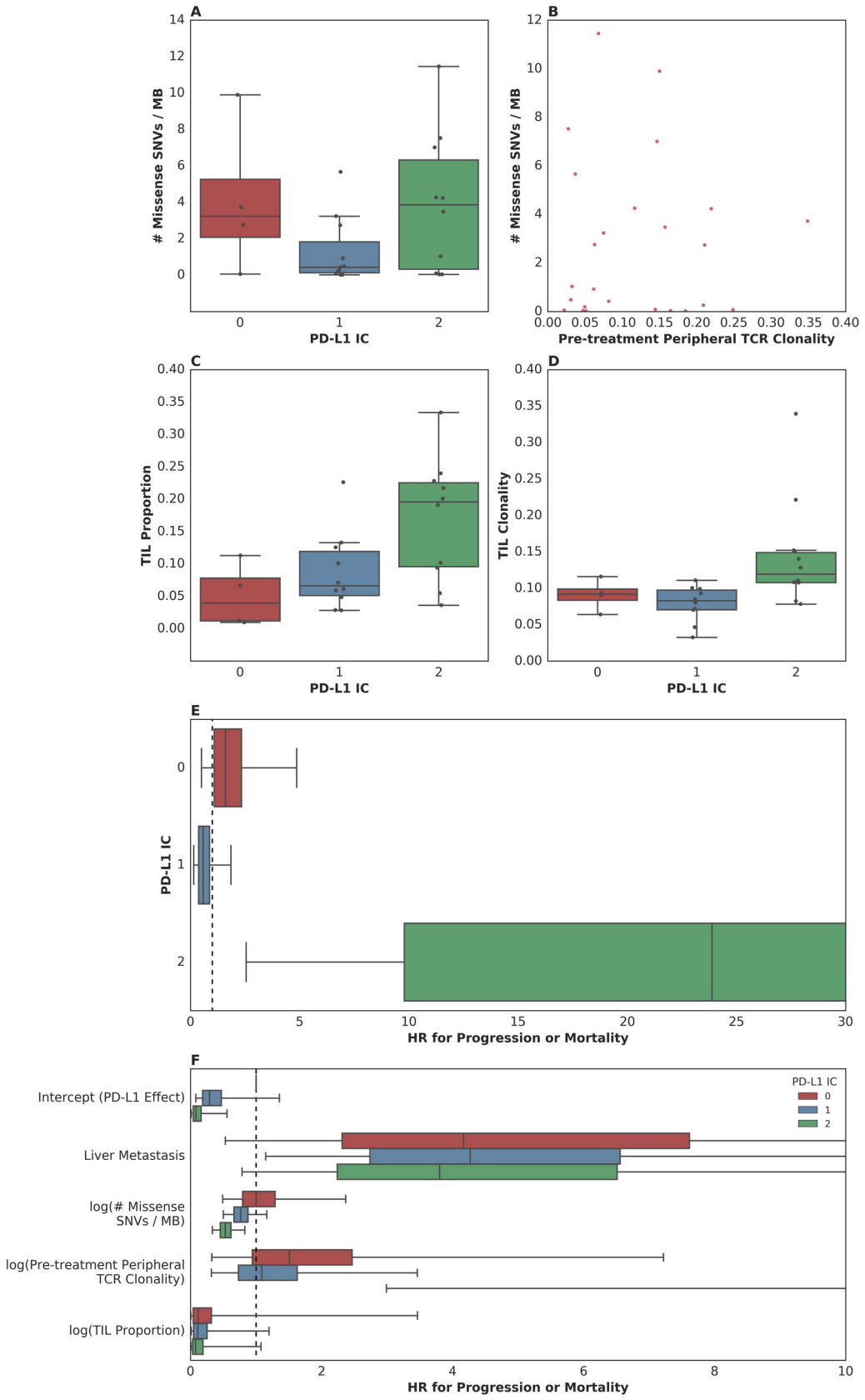
A
Missense SNVs / MB
PD-L1 IC
B
Missense SNVs / MB
Pre-treatment Peripheral TCR Clonality
C
TIL Proportion
PD-L1 IC
D
TIL Clonality
PD-L1 IC
E
PD-L1 IC
HR for Progression or Mortality
F
Intercept (PD-L1 Effect)
Liver Metastasis
log(# Missense SNVs / MB)
log(Pre-treatment Peripheral TCR Clonality)
log(TIL Proportion)
PD-L1 IC
0
1
2
HR for Progression or Mortality